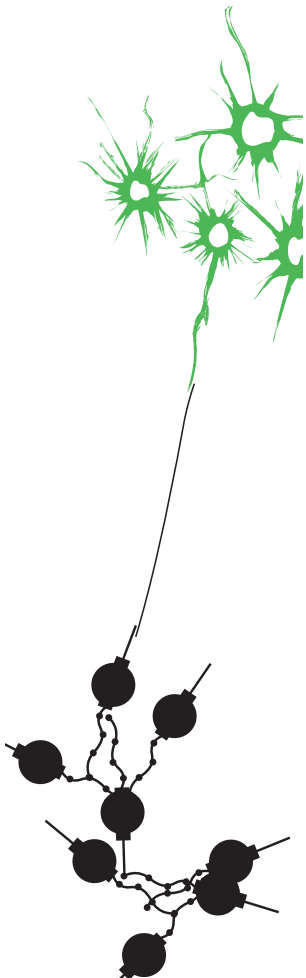

ROBOTICS AND MECHATRONICS

DEVELOPMENT OF A BLADDER PHANTOM OF MATERIALS WHICH CAN BE ANALYSED BY OCT AND A MINIATURE CAMERA FOR THE NEXT-GEN IN-VIVO PROJECT

E.J.A. (Eva) van Beek

BSC ASSIGNMENT

Committee:
dr. F.J. Siepel
dr. V. Groenhuis, MSc
L. Rutten, MSc

July, 2023

034RaM2023
Robotics and Mechatronics
EEMathCS
University of Twente
P.O. Box 217
7500 AE Enschede
The Netherlands

UNIVERSITY OF TWENTE. | TECHMED CENTRE

UNIVERSITY OF TWENTE. | DIGITAL SOCIETY INSTITUTE

Abstract

To improve bladder cancer diagnostics, the Next gen in-vivo project is creating a robot that analyses bladder tissue with optical coherence tomography (OCT) and a miniature camera. A bladder phantom is developed for ex-vivo experiments in the Next gen in-vivo project. OCT is used to visualise possible bladder tumours and the bladder wall. The bladder wall consists of the urothelium, lamina propria and muscularis propria. A miniature camera is used to create a 3D reconstruction of the bladder. The bladder phantom can be analysed with these imaging techniques. Furthermore, the phantom includes blood vessels and tumour sites of the CIS, Ta, T1 and T2 tumours.

Materials and Methods: The techniques sandwich molding and spin coating were used to create the three layers of the bladder wall. A spin coater was developed. Samples were developed to determine which materials were suitable to use in phantoms. Based on the OCT images of the samples, the phantoms were made from Dragon skin and TiO_2. Furthermore, tumours with their characteristics can be created using these materials and analysed with OCT. Different kinds of inks to create blood vessels were tested to determine their influence on the OCT images. Eventually, blood vessels were created using red permanent marker. OCT images of the samples and phantoms and camera images of the second phantom were obtained.

Results: Using sandwich molding and spin coating together with the materials Dragon skin and TiO_2, it is possible to create the three layers of the bladder that can be distinguished with OCT. With these materials the tumours CIS, Ta, T1 and T2 could be developed with certain characteristics and transitions.

Conclusion: To create a bladder phantom with tumours, Dragon skin and TiO_2 were the materials that were most suitable to work with OCT and a miniature camera. The ratio for TiO_2 for the bladder layers are 0.06: 0.21: 0.15 %w/w for the urothelium, lamina propria and muscularis propria respectively. Furthermore, sandwich molding and spin coating were the most suitable techniques.

Samenvatting

Om blaaskanker diagnostiek te verbeteren is het Next gen in-vivo project een robot aan het ontwikkelen die de blaas kan analyseren met optical coherence tomography (OCT) en een miniatuur camera. In het Next gen in-vivo project moet er een blaasfantoom ontwikkeld worden om ex-vivo experimenten uit te kunnen voeren. Hierbij wordt OCT gebruikt om mogelijke blaastumoren en de blaaswand af te beelden. De blaaswand bestaat uit de drie lagen: urotheel, lamina propria en muscularis propria. Daarnaast wordt een miniatuurcamera gebruikt om 3D reconstructies te kunnen maken van de blaas. Met deze twee beeldvormingstechnieken kan het blaasfantoom worden geanalyseerd. Verder bevat het fantoom bloedvaten en tumor locaties van de CIS, Ta, T1, en T2 tumoren.

Materialen en Methoden: Sandwich molding en spin coating zijn de technieken die gebruikt worden voor de samples en fantomen. Hiervoor was een spincoater ontwikkeld. De samples waren ontwikkeld om de meest geschikte materialen voor de fantomen te bepalen. Op basis van de OCT-beelden van de samples waren fantomen gemaakt van Dragon skin en TiO_2. Deze materialen waren ook gebruikt om tumoren te ontwikkelen. Deze kunnen ook met OCT worden geanalyseerd. Verder werden verschillende soorten inkt getest om bloedvaten te creëren om te bepalen welke invloed ze hadden op OCT beelden. Uiteindelijk werden bloedvaten gemaakt van rode permanente marker. OCT beelden van de samples en fantomen waren verkregen. Daarnaast zijn er ook camerabeelden van het tweede fantoom verkregen.

Resultaten: Door gebruik te maken van sandwich molding en spin coating in combinatie met de materialen Dragon skin en TiO_2 is het mogelijk om de drie lagen van de blaas te creëren die onderscheiden kunnen worden met OCT. Daarnaast kon met deze materialen de tumoren CIS, Ta, T1 en T2 worden ontwikkeld met specifieke kenmerken en overgangen.

Conclusie: De materialen Dragon skin en TiO_2 waren het meest geschikt voor een blaasfantoom met tumoren die te analyseren is met OCT en een miniatuur camera. De ratio van TiO_2 voor de blaaslagen is 0.06: 0.21: 0.15 %w/w respectievelijk voor urotheel, lamina propria en muscularis propria. Verder waren sandwich molding en spin coating de meest geschikte technieken voor het ontwikkelen van de blaaslagen.

Contents

1 Introduction **3**

2 Background **4**
2.1 Bladder . . . 4
2.2 Bladder cancer . . . 4
2.3 OCT . . . 5
2.4 Miniature camera . . . 6
2.5 Phantoms . . . 6
2.5.1 Materials . . . 6
2.5.2 Techniques . . . 7

3 Requirements **8**
3.1 Requirements specifications . . . 8
3.2 Suitable materials and techniques . . . 10

4 Materials and Methods **12**
4.1 Materials . . . 12
4.2 Techniques . . . 12
4.2.1 Samples and phantoms . . . 15
4.3 OCT scans . . . 16
4.4 Miniature camera images . . . 17

5 Results **18**
5.1 Spin coater . . . 18
5.2 Samples . . . 19
5.3 Phantoms . . . 21
5.4 Miniature camera . . . 24

6 Discussion **25**
6.1 Materials . . . 25
6.2 Techniques . . . 26
6.3 OCT images . . . 26
6.4 Tumour sites . . . 26
6.5 Phantom suggestions . . . 27
6.6 Further research . . . 27

7 Conclusion **28**

1 Introduction

In 2020, bladder cancer was the tenth most common cancer worldwide [1]. To diagnose bladder cancer, several imaging techniques are used. In the first place, computed tomography (CT), urography or ultrasound can be used, followed by white light cystoscopy (WLC). When histological evaluation is required, a transurethral resection of the bladder (TURB) can be performed [2]. WLC is used to diagnose the tumour in the bladder. A disadvantage of WLC is that the early stage tumours, like carcinoma in situ (CIS), are not detected and it increases the change of recurrence and possible progression of bladder cancer [3]. A different imaging technique that can be used to improve diagnostics of bladder cancer is optical coherence tomography (OCT). This technique is most often based on near-infrared light (890-1300 nm) and is a real time, non-invasive technique. This technique is already used in for example ophthalmology [4]. For further improvement of diagnostics for bladder cancer, the Next gen in-vivo project is developing an OCT-catheter system. In this project robotic systems and software tools are developed for ex-vivo and in-vivo bladder scans and visualisation and assessment of bladder tumours [5]. An OCT probe is used to visualise the anatomy of the bladder wall and of possible tumours [6]. A miniature camera is used for 3D reconstruction of the bladder and location determination [5].

For the Next gen in-vivo project a bladder phantom is needed to perform ex-vivo experiments. To develop this phantom, the following research question based on Chapters 2 and 3 will be answered.
What are suitable materials and techniques for developing a bladder phantom, including tumour sites, that can be analysed with OCT and a miniature camera in the Next gen in-vivo project?
Suitable materials and techniques are based on the following requirements: the phantom should be able to be analysed with OCT and a miniature camera for the Next gen in-vivo project; the phantom should partly resemble the anatomy, physiology and pathology of a human bladder; the phantom should be reproducible on a low budget. These requirements are further explained in Chapter 3.
To meet these requirements, the following sub-questions will be answered. What materials can be used for the development of a bladder phantom with tumour sites that can be used with OCT? What techniques can be used to develop a bladder phantom that partially resembles the anatomy, physiology and pathology of a human bladder? What techniques can be used to analyse a bladder phantom with a miniature camera which does not influence OCT quality?

To develop a bladder phantom, a literary study was conducted on the current phantoms, materials and techniques used for making bladder phantoms. Based on this, requirements were established. The most suitable techniques and materials were selected that met the requirements. Several samples and phantoms were developed and imaged with OCT. In addition, tumour sites were added to the phantoms and analysed with OCT. Furthermore, blood vessels were added that were analysed with a miniature camera to perform ex-vivo experiments.

2 Background

2.1 Bladder

The urinary system consists of the kidneys, ureters, urethra and urinary bladder. The ureters transport the urine from the kidneys to the bladder, where it is stored until the urethra transports it to the exterior of the body. The openings for the ureters and urethra in the urinary bladder lie in the trigone area, see figure 1. So, the role of the bladder in the urinary system is to temporarily store urine. For that function the bladder is quite muscular and can expand to be able to store liquids up to 500 mL comfortably. The maximum storage is 800 to 1000 mL [7]. To be able to achieve the main task of the bladder, it consists of multiple layers. From the inside to the outside these are the urothelium, lamina propria and muscularis propria, see figure 2 [7, 8]. The innermost layer is the urothelium, also known as transitional epithelium [7]. It is a thin layer with a thickness of 50 μm [9]. The lamina propria is made out of many specialised cells, including afferent and efferent nerve endings [8]. Blood vessels are also present in this layer. This layer has a thickness of 150 μm [9].

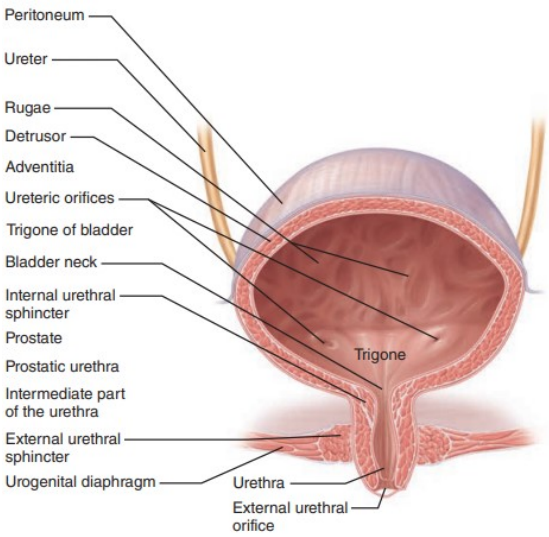

Figure 1: *Urinary bladder of a female [7].*

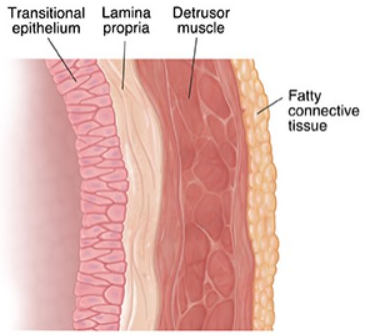

Figure 2: *Layers of the urinary bladder wall [10].*

The muscularis propria, also called detrusor muscle, is a thick, smooth muscle that consists of multiple layers that contract or relax causing movement towards the urethra. When the bladder is completely filled, it is pear shaped and almost smooth from the inside. The emptied bladder is shaped almost pyramid-like and contains many creases on the wall to be able to store enough urine. These creases are able to extend when the bladder volume increases. The surface area of the bladder changes with the amount of stored urine because of these creases [7]. For a small filled bladder with $\sim$ 210 mL, the bladder has a surface area of $\sim$ 200 cm^2 [11]. To store different amounts of urine volumes, the bladder wall needs to be able to stretch. The amount of stiffness of the bladder wall is determined by the Young's modulus. For the wall of the bladder the Young's modulus is in a range of 141-526 kPa, depending on the urine volume present [12, 13].

2.2 Bladder cancer

In 2020, bladder cancer was the tenth most common cancer globally [1]. It was mostly common in people older than 60 [14]. Smoking and exposure to aromatic amines are examples of causes of bladder cancer [2]. There are different types of bladder cancer, urothelium carcinoma is the most common [14]. Several stages of bladder cancer can be identified. In previous research, certain stages have already been imaged with optical coherence tomography (OCT) [4, 15–17]. Stages Ta, T1 and CIS are tumours located only in the urothelium and possibly lamina propria. In stage T2 the tumour invades the muscularis propria [2]. Each tumour stage has its own properties. Stage Ta, also called non-invasive papillary carcinoma, is a tumour that is only present in the urothelium layer and it is visible by a thickened urothelium layer [4, 16]. CIS, carcinoma in situ, is a flat tumour only present in the urothelium layer. It is characterised by only two distinctive layers: the lamina propria and the muscularis propria. The urothelium is not visible. From stage T1 tumours, the cancer is classified as invasive and is present in the subepithelial connective tissue. This is the tissue between the urothelium and lamina propria. It is characterised by only two distinguishable layers.

The muscularis propria is still separate from the two other layers, but the urothelium and lamina propria are not distinguishable anymore [4, 15]. Stage T2 is a muscle invasive tumour and invades the muscularis propria. Subsequently, there is no visible difference between the three layers [2, 4, 15, 16].

2.3 OCT

Optical coherence tomography (OCT) is one of the imaging techniques used in the Next gen in-vivo project to visualize the layers of the bladder wall and possible tumours [5]. It is an imaging technique that creates cross-sectional images. The technique typically uses near infrared (NIR) light on semi-transparent tissues. The light travels in two different paths. One path is reflected by a reference mirror and the second path is created by the backscattering of the light beam from the tissue or sample. The interference of these two paths creates the OCT image. The deeper the light penetrates into the tissue or sample, the more of the light is absorbed and scattered in other directions. These two things make up attenuation, which decreases the amplitude of the backscattered light on the detector. The amount of backscattering of the tissue or sample gives rise to bright or dark regions in an OCT image. OCT imaging is quite fast and images a depth of only a few millimeters [18].

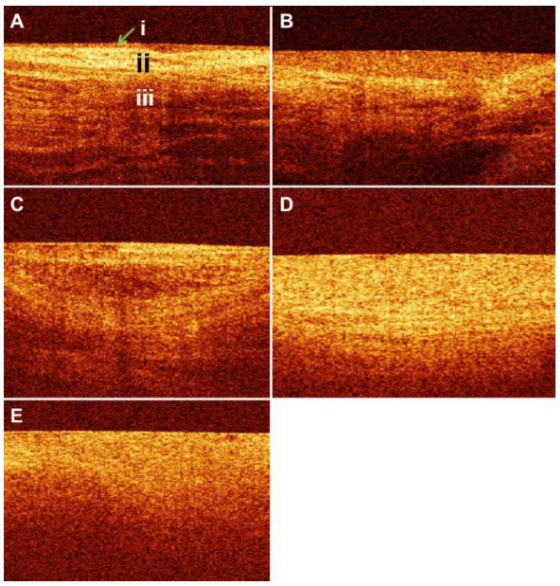

Figure 3: *OCT images of a healthy, human bladder wall and a bladder wall with tumours. (A) Is the healthy wall with a dark thin urothelium (i), a thicker, bright lamina propria and a thick, dark muscularis propria (iii). (B) The Ta tumour with thickened urothelium. (C) CIS tumour, no urothelium is visible. (D) T1 with thick, combined urothelium and lamina propria layer. And (E) the T2 tumour with no distinguishable layers [4].*

There are two types of scans that can be created using OCT: the B-scan and C-scan. The base of both scans is the A-line. This is the signal that is acquired by the reflectivity of the sample, depending on the depth the light penetrates the sample that still gives backscattering. If many A-lines are positioned successively, a two dimensional B-scan is created. This can be achieved by scanning in one line over the sample. By scanning in a square for example, a three dimensional scan can be made, called a C-scan [18].

The bladder can be imaged by the OCT technique to improve the diagnosis of bladder cancer. The three layers of the bladder, urothelium (i), lamina propria (ii) and muscularis propria (iii), are distinguishable on an OCT image, see figure 3A . Each layer has it's own optical properties [4]. On an OCT image the urothelium is the layer visible with the least intensity, the lamina propria has the highest intensity and the muscularis propria has an intensity between those two other layers [4, 16]. Different bladder tumours can be visualised with OCT. In figure 3 the tumour types Ta (B), T1 (C), CIS (D) and T2 (E) are depicted. Each tumour has its own characteristics as discussed in paragraph 2.2 [4].

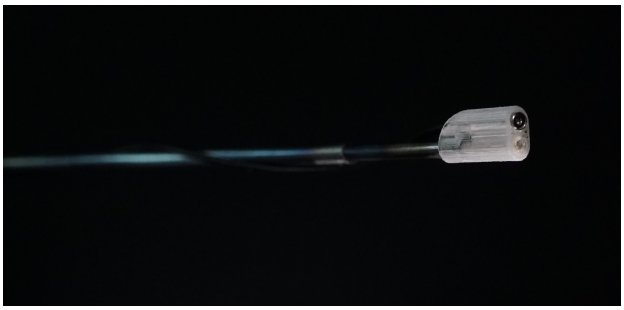

Figure 4: *Catheter of end-effector of robot in Next gen in-vivo project with OCT (below) and miniature camera (top).*

2.4 Miniature camera

The second imaging technique used in the Next gen in-vivo project is a miniature camera. This camera is located in the catheter of the end-effector (see the top of the catheter in figure 4). On the bottom is the OCT probe that will be used to image the layers of the bladder phantom, as discussed in paragraph 2.3.
The camera is used to show the location and range that can be visualised with the catheter. The camera only shows the surface and does not image in the depth of the bladder wall like OCT does. The camera images are made with lights on in the surrounding environment. The images can be compared to the commonly used diagnostic imaging technique for bladder cancer: white light cytoscopy (WLC). Several characteristics of the bladder are visible with WLC, e.g. blood vessels and subtle appearance of several tumours, see figure 5 [19]. This can possibly be visualized with the miniature camera. Early staged tumours like CIS or other small, papillary lesions are difficult to diagnose with WLC, because it does not show the different layers in the bladder wall [19, 20].

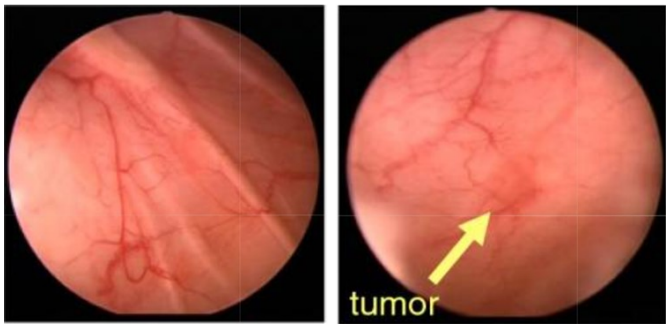

Figure 5: *WLC images of healthy bladder tissue (left) and tumorous tissue (right) [19].*

2.5 Phantoms

Phantoms of different tissues have already been developed for many organs, like the colon, the retina or the bladder [21–26]. Currently, several bladder phantoms exist that can be analysed by OCT [19, 24–28]. Different kinds of materials and techniques have been used to create these bladder phantoms, several will be discussed in this paragraph.

2.5.1 Materials

Materials used for phantoms of organs analysed with OCT need to have specific properties, like certain optical, mechanical, structural and stabilising properties [29]. Phantoms of a bladder need to have a certain Young's modulus (around 141 to 526 kPa [12, 13]) and contain the three layers of the bladder wall [7] for example. In addition, the base material, which a phantom is primarily made of, needs to be optically tunable to allow the phantom to be used with specific imaging techniques. The optical properties are then determined by a scatterer that is added to this base material [29].

Different materials have been used to fabricate a phantom of human organs, like polyvinyl chloride-plastisol (PVCP), hydrogels or silicones. Each category of materials has its own advantages and disadvantages [29]. Starting with polyvinyl chloride-plastisol (PVCP). This is a material that is optically and acoustically well tunable, as it is optically transparent after preparation [29]. This material has not yet been used for bladder phantoms, but can be used for organ phantoms, like a skin phantom [30]. In addition, PVCP is stable for $\sim$6 months [29].
Secondly, another material are hydrogels. There are different types of hydrogels. The ones used for phantoms of the urinary system are agar, gelatin and PVA [27, 31]. Agar and gelatin are known for their easy production and compatibility with organic materials. However, some disadvantages are that these materials are prone to mould, breakage and dehydration. Consequently, agar and gelatin can only be stored for a couple of weeks [29]. PVA (Polyvinyl alcohol) is a hydrogel as well but with a longer shelf life of 6 months. Different

properties, like mechanical and optical properties, are difficult to alter separately during the fabrication of this material [29, 32].
Silicone is another commonly used material for bladder phantoms [29]. There are different kinds of silicones, like PDMS (polydimethylsiloxane), Ecoflex and Dragon skin. PDMS is one of the most used silicones in bladder phantoms [19, 25, 28]. The PDMS Sylgar 184 elastomer is the most used type and can be used with many different techniques, like sandwich molding, spin coating, airbrushing or painting [19, 25, 28]. These techniques will be discussed in paragraph 2.5.2. The curing time of PDMS is around 30 minutes and the shelf life is several years. PDMS has a Young's modulus of 800 kPa - 1.72 MPa [24]. Another material used for bladder phantoms is Ecoflex. This silicone rubber material has been used with a molding technique [26]. There are many different kinds of Ecoflex that differ in hardness, curing time (from 5 minutes to 4 hours) and other properties that vary per type of Ecoflex [33]. The Ecoflex used in the research of Choi et al [26] was Ecoflex 00-20 that had a Young's modulus of approximately 55 kPa. Finally, Dragon skin, a silicone rubber with a Young's modulus of 150 - 593 kPa, has a curing time of 30 minutes to 7 hours [24]. It also has a varying amount of hardness per type of Dragon skin [34]. In the research of Smith et al [24] Dragon skin was used with airbrushing.

Scatterers are used in most phantoms to be able to optically tune the image for required properties. Metal oxide powders are used as scatterers in bladder phantoms. TiO_2, silica gel (SiO_2) or AlO_3 are commonly used [19, 24, 25, 27–29]. TiO2 has a relatively high refractive index of 2.49, which is higher than that of silica gel which is 1.37 at a wavelength of 589 nm. [22] With a higher refractive index less material is usually needed for the same amount of influence on the optical properties.

2.5.2 Techniques

Several techniques exist that can be used to develop tissue like phantoms in 3D. These techniques vary in procedure and desired outcome. The techniques sandwich molding, painting, air brushing and spin coating will be discussed to create the base of the bladder phantom. In addition, the techniques inking, extrusion and embossing will be shortly touched upon. These techniques are used to add further details to the phantom.

One of the more commonly used techniques in bladder phantoms is sandwich molding [19, 24, 26]. This is a technique where the material is 'sandwiched' together between an inner and outer mold. These molds are usually 3D printed. There is a big variety of shapes that can be achieved with this technique. Additionally, most materials are degassed to prevent air bubbles in the material. A disadvantage is that only layers thicker than 250 μm can be created [19]. Painting is also a technique that is used to create bladder phantoms. The material is poured on the desired container and spread out with a spatula [28]. This technique can be used to make complex 3D shapes and thin layers can be created, but it is difficult to control the thickness of the layers across the entire phantom [24, 28]. Thirdly, air brushing is a technique used for producing bladder phantoms [24, 25]. The material that is used with this technique should be viscous enough to be able to airbrush or materials should be added to make them more viscous. Thin, uniform layers can be created and complex 3D shapes can be fabricated as well [24]. Another technique to be able to create thin layers is spin coating. The material is rotated in a mold on high speeds to create homogeneous layers, the higher the speed, the thinner the layers. When the speed is too low hypercoating can occur, where material piles up. Or when the speed is too high, hypocoating can occur: the material does not stick and covers the mold badly [19].

The following techniques are used for further details on the phantoms. Firstly, to create blood vessels on the bladder phantom different techniques can be used. Inking can be used to draw the required blood vessels on the phantom [19]. Next to that, it is possible to place pieces of cord on the uncured material and remove them afterwards [24]. Secondly, to create tumour sites, excision is possible. This is done by the excision of regions and then by filling these regions up to recreate desired layers with their own characteristics [19, 24]. Finally, embossing is used to mimic the creases in the bladder wall [7]. Often crumpled (aluminium) foil is added before the base material is cured to create a rough surface [19, 24, 25, 28].

3 Requirements

In order to select suitable techniques and materials to develop a bladder phantom, several requirements need to be determined. Functional requirements are established for the expectations of the bladder phantom. These functional requirements are extended to technical requirements to measure the functional requirements.

3.1 Requirements specifications

The functional requirements for a bladder phantom are that the phantom can be used in the Next gen in-vivo project, because the bladder phantom is used for ex-vivo experiments in this project. A bladder phantom should closely resemble the anatomy, physiology and pathology of a human bladder. Lastly the phantom should be reproducible on a low budget to be able to reproduce the phantom and still make changes if needed after development.
Technical requirements are established for each functional requirement in order to measure them. Table 1 outlines both types of requirements. The technical requirements are further specified to be able to quantify them. Furthermore, it is specified that the technical requirement is either a wish (W) or a requirement (R). Wishes are implemented when there is room to apply these. Moreover, the wishes and requirements are rated for importance with a number from 1 (least important) to 10 (most important). And lastly, it is stated whether the requirement was finally met (✓), partially met (∼) or not tested (×).

Table 1: Overview of functional and technical requirements specified if they are either a wish (W) or requirement (R) and rated on a scale from 1 (least important) to 10 (most important). And stated if the requirement was met (✓), partially met (∼) or not tested (×).

Label	Requirements	Specifications	R/W	Rate	(Not) met
FR1	**Phantom can be used in Next gen in-vivo project.**				
TN1	The catheter should be able to reach inside the phantom.	To be able to make images of the inside of the phantom with either OCT or miniature camera.	R	9	✓
TN2	Visible layers on OCT.	OCT is on of the imaging techniques used in the Next gen in-vivo project. Layers need to be distinguishable.	R	10	✓
TN3	Can be used with the miniature camera.	This is an imaging technique used in the Next gen in-vivo project.	R	5	✓
TN4	Phantom can be preserved for at least 2 year.	A shelf life of at least 2 years is needed to reuse the phantom for experiments. This shelf life includes mechanical and optical properties of the phantom.	R	7	✓
FR2	**Phantom resembles anatomy of a human bladder.**				

Continued on next page

Table 1: Overview of functional and technical requirements specified if they are either a wish (W) or requirement (R) and rated on a scale from 1 (least important) to 10 (most important). And stated if the requirement was met (✓), partially met (∼) or not tested (×). (Continued)

TA1	Anatomy of the three inner layers of the bladder wall.	The bladder wall consists of 3 uniform layers: 2 thinner urothelium and lamina propria and 1 thicker muscularis propria [7].	R	7	✓
TA2		The first two layers of the bladder wall should have a thickness of 50 μm and 150 μm for the urothelium and lamina propria respectively [9].	R	6	∼
TA3	Size of the bladder.	For realistic ex-vivo experiments. Default is a low volume state of the bladder of ∼ 200 mL with a surface area of ∼ 200 cm^2 [11].	W	4	✓
TA4	Shape of bladder.	For realistic ex-vivo experiments. The bladder should be pyramid shaped when almost empty [7].	W	3	×
TA5		Bladder should be whole with two holes for the urethra and ureters [7].	W	3	×
TA6	Opening for urethers and urethra.	To be able to include fluids in the phantom for ex-vivo experiments. 2 urethers and 1 urethra opening [7].	W	2	×
TA7	Phantom is hollow.	The main function of the bladder is to hold fluids [7].	R	8	✓
TA8	Blood vessels and nerves visible.	For a realistic bladder phantom and should be visible on a miniature camera.	W	5	∼
TA9	Creases on the inside of the bladder wall.	This is a characteristic of the bladder wall to be able to store more urine [7].	W	5	×
FR3	**Phantom resembles physiology of a human bladder.**				
TPH1	Phantom should be able to contain fluids.	This is the main function of the bladder [7].	W	2	×
TPH2	Phantom has elastic properties.	Phantom should have a Young's modulus between 140-526 kPa [12, 13].	R	6	∼
FR4	**Phantom resembles pathology of a human bladder.**				

Continued on next page

Table 1: Overview of functional and technical requirements specified if they are either a wish (W) or requirement (R) and rated on a scale from 1 (least important) to 10 (most important). And stated if the requirement was met (✓), partially met (∼) or not tested (×). (Continued)

TPA	Bladder cancer of types CIS, Ta, T1 and T2 visible in phantom.	Common bladder cancer tumour that can be analysed with OCT [4, 16].	W	6	✓
FR5	**Phantom should be reproducible on a low budget.**				
TR1	Affordable and easily accessible materials.	Both silicone rubber and scatterer should be affordable and easily accessible for remaking and further development of the phantom. Easily accessible means that it is available at RaM or possible to order online.	R	7	✓
TR2	Easy accessible techniques.	To be able to remake and/or further development of the phantom. Easily accessible means that it is available at RaM or possible to order online.	R	8	✓
TR3	Relatively easy procedure to make the phantom.	It should be possible to remake the phantom in approximately 1 day. This includes preparations, procedure and curing time.	R	6	✓

3.2 Suitable materials and techniques

For the development of the bladder phantoms, suitable techniques and materials should be used that meet the above requirements. The materials and techniques discussed in this paragraph are based on paragraph 2.5.1.

According to requirement TN4 the phantom should have a shelf life of at least two years. As explained in paragraph 2.5.1, hydrogels cannot meet this requirement, because agar and gelatin have a shelf life of only a couple of weeks and PVA a shelf life of 6 months. Moreover, PVCP has a shelf life of 6 months as well and therefore does not meet this requirement [29]. PDMS, Dragon skin and Ecoflex comply with this requirement, since they have a shelf life of several years [24]. Both Ecoflex and Dragon skin are easily accessible since they can be ordered online and are both affordable, which meets requirement TR1. The affordability part of this requirement does not apply to PDMS and therefore it will not be used. There are different types of Dragon skin, including ones that have quite short curing times [34], which has an impact on requirement TR3. Furthermore, Dragon skin has a Young's modulus of 150 - 593 kPa [24], which corresponds with requirement TPH2. The second material used is Ecoflex. This material also has various curing times that are workable in 24 hours [33], which corresponds with requirement TPH2.

TiO_2 and silica gel are used for scatterers. Both materials were already available at RaM or easy to order, meeting requirement TR1. Next to that, both materials can be used to optically tune silicone material [29], therefore meeting requirement TN2 and TPA.

Suitable techniques for creating the thicker muscularis propria layer (requirement TA1) are sandwich molding, painting or multiple spin coating layers. Sandwich molding is preferred because this technique makes consistent layers, which is not easily possible with painting [24, 28]. Furthermore, sandwich molding only needs one layer to cure, to create a thick layer, compared to making and curing multiple layers with spin

coating. Therefore sandwich molding meets requirement TR3. Lastly, sandwich molding meets requirement TR3 as well since only two molds are needed (inner and outer mold), which can be 3D printed.
To create thin layers airbrushing, painting and spin coating are suitable techniques. Spin coating will be used, because it gives consistent layers unlike painting [24, 28]. In addition, with airbrushing uniform layers are difficult to obtain as well. Furthermore, a certain consistency is required that does not clog the airbrushing device. [24]. Therefore, spin coating meets the requirement TA1. Lastly, a spin coater was not available at RaM, but it was possible to built one with the materials present at RaM, therefore meeting requirement TR2.
Together with the preparation, process and curing times for 3 layers of the materials, it should be possible to remake the phantom in 24 hours with sandwich molding and spin coating, which meets requirement TR3.

4 Materials and Methods

Several techniques and materials were used to create various samples and phantoms. The techniques sandwich molding and spin coating were used to create five pairs of samples and two phantoms. The phantoms contain tumour sites and blood vessels. Both samples and phantoms were analysed with an OCT system and the phantoms were analysed with a miniature camera to visualise the blood vessels.

4.1 Materials

As discussed in paragraph 3.2, Dragon skin, Ecoflex, TiO_2 and silica gel were materials that meet the requirements set in paragraph 3.1. The specific materials used for both the samples and phantoms will be discussed in this paragraph.

The samples were made of Dragon Skin 10 NV (Smooth-on) and Ecoflex 00-30 (Smooth-on) as silicone rubber material. Titanium(IV) oxide, anatase (Sigma Aldrich) and Silica gel 60-200 μm (VWR chemicals) were used as scatterers. For the bladder phantoms, only Dragon skin 10 NV and Titanium(IV) oxide, (also called TiO_2) were used.
Dragon skin 10 NV is a skin safe silicone rubber with a pot life of 15 minutes and a curing time of 75 minutes [35]. This type of Dragon skin was preferred because of a relative short but still workable pot life. In 15 minutes there was enough time for the execution of the instruction steps before the material started to cure. Dragon skin was prepared according to the instructions of the supplier (Smooth-on [35]) with an extra addition of vacuum degassing for the muscularis propria layer, although this was not necessary according to the supplier. This was done because there were air bubbles present in the first samples.
The other silicone material used was Ecoflex 00-30. It is a stiffer material than the Dragon skin 10 NV. Moreover, it has a pot life of 45 minutes and cure time of 4 hours. It was preferred over Ecoflex 00-10 because it can be more elongated (900% vs 800%) and is stronger than Ecoflex 00-10 with the same kind of preparation. And Ecoflex 00-30 had a softer shore hardness than Ecoflex 00-50 and was therefore more preferred [33]. This material was prepared exactly according to the instructions of the supplier (Smooth-on [33]).

To be able to see the different layers of the bladder wall on an OCT system, scatterers were added to influence the optical properties. These scatterers were TiO_2 and silica gel. Two ratios were tested for TiO_2 and one ratio for silica gel. The first ratio used for TiO_2 was used in the research by Lurie et al. [19] and was 0.06: 0.21 : 0.15 %w/w for the urothelium, lamina propria and the muscularis propria respectively. The second ratio of TiO_2 and the ratio of silica gel were based on the research by de Bruin et al. [22] and Ejofodomi et al. [36] together. The ratio used for TiO_2 was 0.02 : 0.1 : 0.07 %w/w and for silica gel it was 0.09 : 0.45 : 0.31 %w/w for the urothelium, lamina propria and muscularis propria respectively.

4.2 Techniques

As discussed in paragraph 3.2 both sandwich molding and spin coating were techniques used to create layers. Sandwich molding was a good technique for creating thick layers for the muscularis propria. This was done by using 3D printed sample and phantom molds. To create thinner layers for the urothelium and lamina propria spin coating was used. A spin coater was created for this. Furthermore, tumour sites and blood vessels were added to the phantoms.

Sandwich molding (inner and outer mold) and spin coating (only outer mold) both required molds. These molds were created using an Ultimaker S5 3D printer. Both sample and phantom molds were based on spheres to prevent hypercoating or hypocoating. One set of inner and outer molds were made for the samples, called lower bladder sample molds, based on a spherical cap of a sphere with a diameter of 65.6 mm which was based on a sphere with a volume of 500 mL. The difference in inner and outer mold and thereby thickness of the muscularis propria layer was 1.4 mm. These sample molds were made of Polyactic acid (PLA) material with a print core AA 0.4, printed with a resolution of 0.15 mm.

A rectangular shaped container (9x4 cm) was used to make the rectangular samples. These were created as a back-up to still be able to make OCT-images of the different materials if there would be something wrong with the lower bladder samples, like breakage, spin coater errors (hypercoating and hypocoating) etc. The rectangular samples and lower bladder samples (spherical caps) were created at the same time and therefore have the same material properties. For the layers of the rectangular samples, first the volume was calculated that was needed for a certain thickness (lxwxh). The material was poured into the container and with a little piece of flat wood that fitted into the container the material was flattened out, called painting.

A second set of inner and outer molds were produced for the bladder phantom, called phantom molds. The outer mold had a diameter of 80 mm that was based on a the surface area of the bladder filled with $\sim$ 210 mL to be able to stretch for more [11]. This stretch happens when the bladder would be filled with bigger volumes. The gap between the inner and outer mold was 1.75 mm. These phantom molds were both made out of Though PLA with a AA 0.4 print core. The inner mold was printed with a resolution of 0.1 mm to reduce the saw teeth visible with a resolution of 0.15 mm. This mold was sanded smooth with sandpaper as well to further reduce the saw teeth. The outer mold was printed with a resolution of 0.15 mm. The separate molds are visible in figures 6a and 6b. The molds assembled with a visible gap are shown in figure 6c.

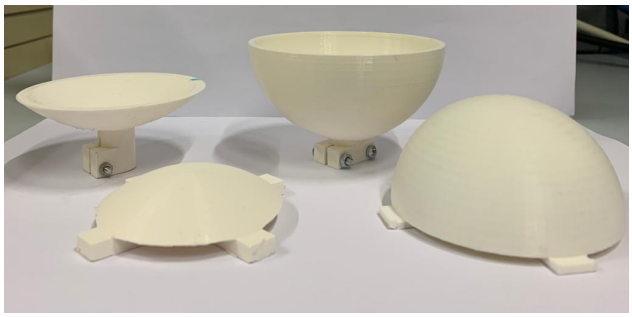

(a) Side view of inner and outer molds of sample molds (left) and phantom molds (right).

(b) View form above of inner and outer molds of sample molds (right) and phantom molds (left).

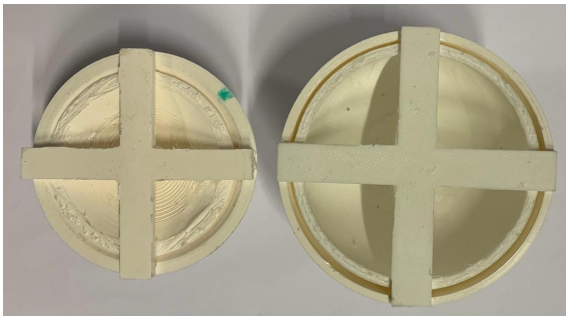

(c) Molds assembled, visible space between inner and outer molds of sample molds (left) and phantom molds (right).

Figure 6: *Inner and outer molds of sample molds and phantom molds.*

For sandwich molding both inner and outer molds were used for both the sample and phantom molds. Sandwich molding instructions for both silicone materials and scatterers were in short:

1. Check if setup is level.

2. Mix parts A and B of the silicone rubber with 1:1 ratio of the desired amount.
3. Add desired amount of scatterer to the mixture.
4. Mix mixture thoroughly for 3 minutes.
5. Put the mixture in vacuum degasser until flat surface (for Ecoflex 1 minute longer after surface is flat).
6. Place inner mold on outer mold. Pour mixture into space between inner and outer mold without lifting inner mold to prevent air bubbles.

To create thin layers, spin coating was used. A spin coater was built from a stand, an unidentified electro motor, a power supply (Delta Elektronika Zierikzee), 2 measuring cups and the outer molds of sample and phantom molds, see figure 7 for the phantom setup for sandwich molding (left) and spin coating (right). The difference between the setups is that the attached inner mold was removed in the spin coating setup. For all experiments the power supply was set on maximum current.
For both the sample and phantom setups the spin speeds were determined for different voltages. This was done using a piece of tape and a stopwatch. The rounds that the mold made were counted and using the time on the stopwatch the rounds per minute (rpm) were calculated. Then the slope of the trendline acquired by the data points was calculated.
After the OCT scans of the samples (see paragraph 4.3) the thickness of the lamina propria and urothelium, using the measuring tool in Microsoft PowerToys, were estimated. This was represented in a graph and a slope of the trendline was calculated which was used together with the slopes of the voltage and spin speeds graphs to estimate the required voltages for the lamina propria and urothelium layer in the phantoms.
The lamina propria and urothelium layers were created using spin coating. The first 4 steps of the instructions from sandwich molding were used for spin coating as well. Following instructions applied for the spin coating steps:

5. Pour mixture into the middle of the outer mold.
6. Place measuring cups around electro motor and mold.
7. Turn power supply on with maximum electric current and desired voltage, visible in table 2.

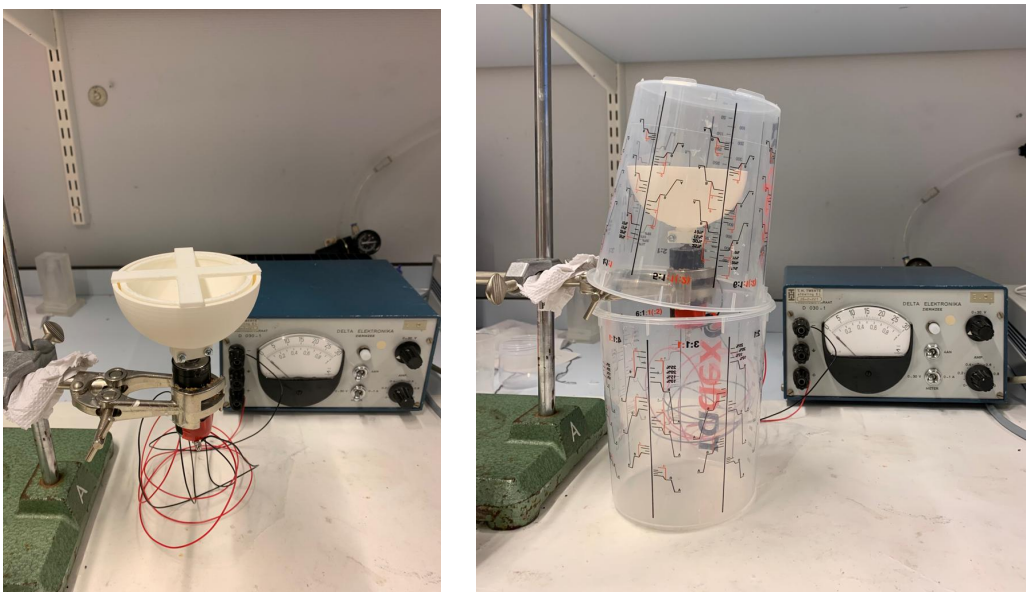

(a) Side view of setup for sandwich molding. Setup is levelled.

(b) Side view of setup for spin coating. Electro motor is attached to the power supply.

Figure 7: *Setups for both sandwich molding (a) and spin coating techniques (b).*

4.2.1 Samples and phantoms

A total of five pairs of samples and two phantoms were made. Every pair of samples consists of a spherical cap representing the lower part of the bladder and a flat rectangle with the same properties and therefore same label colour. Between every sample one thing was changed, either the silicone rubber, the scatterer (ratio) or the power supply voltage, visible in table 2. The phantoms were made out of the same materials. In phantom BP2 the best techniques for creating tumours in phantom BP1 were used. For the tumours and techniques, see table 3.

Table 2: *Labels, materials, scatterers, ratios of the scatterers and voltages of spin coater of the five pairs of samples (DST1 - EFT) and the two phantoms (BP1, BP2). The urothelium (U), lamina propria (LP) and muscularis propria (MP) have different ratios of scatterers.*

Label	Colour	Material	Scatter	Ratio (%w/w) (U:LP:MP)	Voltage (V) (U:LP)
DST1	Green	Dragon skin 10 NV	TiO_2	0.06 : 0.21 : 0.15	4 : 1.7
DST2	Pink	Dragon skin 10 NV	TiO_2	0.06 : 0.21 : 0.15	4 : 2
DST3	Yellow	Dragon skin 10 NV	TiO_2	0.02 : 0.1 : 0.07	4.5 : 2.5
DSS	Blue	Dragon skin 10 NV	Silica gel	0.09 : 0.45 : 0.31	5 : 2.1
EFT	Purple	Eco flex 00-30	TiO_2	n.a. : 0.21 : 0.15	n.a. : 2
BP1	n.a.	Dragon skin 10 NV	TiO_2	0.06 : 0.21 : 0.15	4.6 : 3
BP2	n.a.	Dragon skin 10 NV	TiO_2	0.06 : 0.21 : 0.15	4.4 : 2.9

In both phantoms, tumour pieces were added. In phantom BP1 several techniques were tested and the techniques that gave the smoothest look were used in phantom BP2. For the T1, Ta and CIS tumours that are only present in the urothelium (and lamina propria) certain locations of the phantom were covered by layered pieces of tape on the muscularis propria and lamina propria to create little holes. These holes were in the lamina propria or urothelium layers respectively. These holes were then filled up with materials with the desired optical properties with different techniques and excess material was taken of with paper to flatten the tumour. The first technique was making a cutout in a piece of tape the size of the hole that was placed around the previous one and this was filled up with desired material and flattened. A second technique was that the hole was filled up and a complete piece of tape covered the hole pressing out the excess. Lastly, it was tested if the process could be sped up by making two tumours at the same time instead of one. For the T2 tumour, excision was performed, and this hole was filled up with a gradient starting with 0.15 %w/w topped with 0.18 %w/w material. In phantom BP2, the fill up and flatten technique was used for all tumour sites. The same ratios of the scatterers were used as in BP1. An overview of the labels and techniques are visualised in table 3.

In phantom BP1 different kinds of inks were tested that could be used to create blood vessels. These inks should not be visible on the OCT image, because they were only used for the miniature camera. Green ink used for colouring silicones was tested and black and red permanent markers (HEMA, 2mm) were tested. OCT images were analysed to see if the inks influenced the OCT data.

Table 3: *Overview of tumours and their properties added in phantom BP1 (labels WT-PT) and phantom BP2 (labels BS1-BS4). Characteristics of the urothelium (U) and lamina propria (LP) are briefly explained for each tumour.*

Label	Colour	Tumour	Ratio (\%w/w)	Tape location/ extruded	Filling technique	Tumour characteristics
WT	White	T2	0.18:0.15 gradient	Extruded	Filled up and flattened at same time as ZT.	Indistiguishable layers.
ZT	Black	T1	0.18	LP	Cut out square tape around tumour location filled up and flattened at same time as WT.	U and LP indistinguishable.
BT	Dark blue	Ta	0.06	U	Filled up and flattened.	Thick U layer.
RT	Red	CIS	0.21	LP	Filled up and flattened at same time as OT.	No U layer.
OT	Orange	CIS	0.21	U	Filled up and flattened at same time as RT.	No U layer.
PT	Light pink	T2	0.18: 0.15 gradient	Extruded	Tape over filled up tumour location.	Indistiguishable layers.
BS1	n.a.	CIS	0.21	LP	Filled up and flattened.	No U layer.
BS2	n.a.	T1	0.18	LP	Filled up and flattened.	U and LP indistinguishable.
BS3	n.a.	T2	0.18: 0.15 gradient	Extruded	Filled up and flattened.	Indistinguishable layers.
BS4	n.a.	Ta	0.06	U	Filled up and flattened.	Thick U layer.

4.3 OCT scans

The robot that is being created in the Next gen in-vivo project uses two imaging techniques, OCT and miniature camera. With OCT the layers (urothelium, lamina propria and muscularis propria) of the bladder wall and tumours in this wall can be analysed. OCT scans were made of the five lower bladder samples and the two phantoms. The different kinds of materials in the samples (see table 2) were analysed. In the phantoms the layers, tumour sites and inks were analysed. Scinvivo is one of the partners of the Next gen in-vivo project that is making the prototype OCT catheter and part of the prototype OCT catheter system. [5]. This system consist of an OCT probe attached to a 3D-printer frame to be able to make ex-vivo images easily, see figure 8. The field of view of this setup is 5 mm and has a scanning depth of $\sim$ 2 to 3 mm [6]. B-scans were made of all lower bladder samples and of both phantoms. C-scans were made of the BP2 phantom

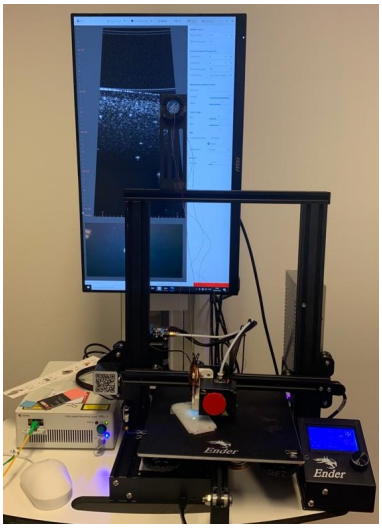

Figure 8: *OCT system made by Scinvivo.*

on all tumour sites and in the middle of the phantom. The settings of the OCT system for both B- and C-scans are presented in table 4. The parameter steps for the settings of the C-scan steps were 10 steps for the CIS and T1 locations and 20 steps for the T2, Ta locations and the normal scans. For the calibration of the system several parameters were determined and vary per scan moment, like the settings for the MEMS mirror, the input range and the exposure of the camera, these vary per calibration. These parameters are not visible in the table.

Table 4: *Settings and parameters for B-scans and C-scans. On the left the settings for both B- and C-scans and on the right settings used for C-scans only.*

Use subsequent B-scans for	
Interlacing	2x
Averaging	4x
Moving averages	Off
Consolidation	Accurately located
Anistropic diffusion filter	
Iterations	0
Lambda	0.25
Kappa	30
Plot	
Coordinate system	Polar
Interpolation	Scinvivo

C-scan steps	
Steps	10 or 20
Pitch	0.1 mm
Angle	110 degrees
Perpendicular steps	
Steps	5
Pitch	1 mm

4.4 Miniature camera images

In the Next gen in-vivo project the second imaging technique, in addition to OCT, is camera recordings. This measures the range that the catheter of the robot can rotate and is able to see the approximate location inside the bladder. The acquired images can be used to make a 3D reconstruction of the bladder.
The images were obtained for the blood vessels and tumours in phantom BP2. The images were made with an Ultra mini CMOS color camera, type FXD-VB20903L-76. The resolution of the images was 1280 x 720 pixels. The camera and cable were inserted in a 3D stand, see figure 9. The camera was plugged in a laptop with USB 2.0 and using the Windows camera program images were obtained.

Figure 9: *Miniature camera used to image blood vessels on phantom BP2.*

5 Results

The results of the spin speeds of the spin coater, the OCT images of the samples and phantoms and the images of the miniature camera of phantom BP2 will be analyzed in this Chapter.

5.1 Spin coater

Using the power supply of the spin coater, the spin speeds of the sample and phantom setups were estimated. Four voltages were tested for each setup, these points were visualised in a graph to represent the correlation of the voltages (V) and spin speeds (rpm), see figures 10 and 11. For the sample setup the trendline had a slope of 318.93 rpm/V, see figure 10.

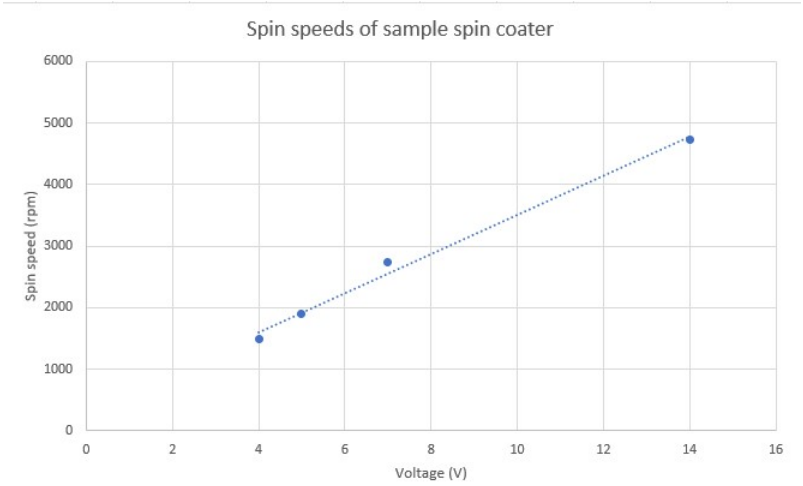

Figure 10: *For different voltages (in V), spin speeds (in rpm) were determined for the sample setup. The trendline has a slope of 318.93 rpm/V.*

For the phantom setup the spin speeds for four different voltages were calculated. This setup had a trendline with a slope of 413.44 rpm/V, see figure 11.

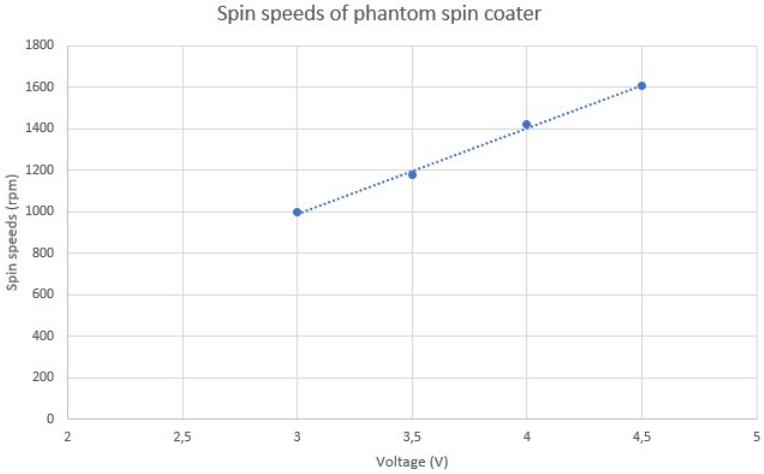

Figure 11: *For different voltages (in V), spin speeds (in rpm) were determined for the phantom setup. The trendline has a slope of* 413.44 *rpm/V.*

5.2 Samples

Five pairs of samples were created, see figure 12. Each pair consists of a lower bladder sample made with spin coating and sandwich molding with a corresponding rectangular sample made with painting, both made with the exact same materials, see table 2. Each pair consists of a different combination of material, spin speeds or scatterer ratio, see table 2. Of each lower bladder sample a B-scan was made with the OCT system of Scinvivo, see figure 13.

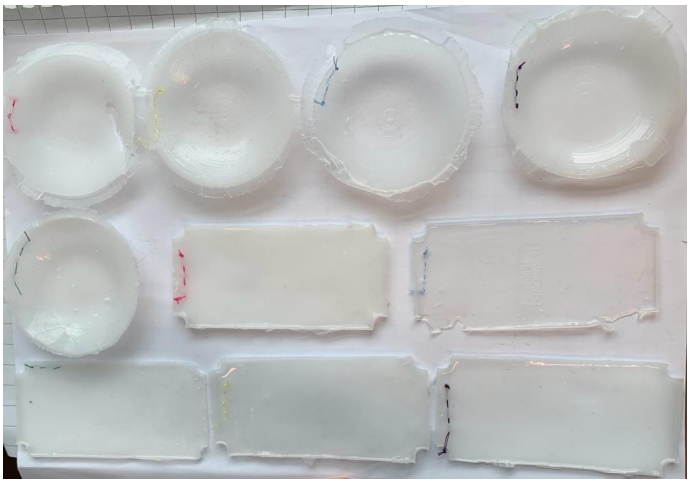

Figure 12: *Overview of all lower bladder samples and corresponding rectangular samples.*

All images in figure 13 include several artefacts and certain characteristics of the setup, see figure 13a. In all samples, except for DSS, a saw tooth pattern is visible, caused by the inner 3D printed mold. The patterns are visible between arrows 3 and 4 in figure 13a. In addition, indicated with arrow 2, all samples show horizontal artefacts that are caused by the OCT probe. Furthermore, another artefact visible in all samples are the bright dots at the top and bottom of the phantom, called the air-tissue interface artefact [37], indicated with arrows 1 and 5. Lastly, in all samples a layer is visible below the phantom (location 6) that represents the tape that is used for the calibration of the OCT system. Arrow 3 indicates the thin layered, low intensity urothelium. Arrow 4 indicates a thicker, more intense lamina propria. The medium intensity part between arrows 4 and 5 indicate the muscularis propria.
The DST1 sample shows two separate layers, a separate urothelium layer is indistinguishable from the lamina propria, see figure 13b. Therefore, the urothelium thickness could not be measured. In this sample the 3D printed inner mold layers are clearly visible as saw teeth.
In the DST2 sample the urothelium, lamina propria and muscularis propria are distinguishable, see figure 13c.
For the DST3 sample the urothelium, lamina propria and muscularis propria are distinguishable but less visible than in DST2, as seen in figure 13d.
The DSS sample does not show any separate layers, it does show all the artefacts.
The EFT sample shows the two separate layers of the lamina propria and the muscularis propria, as expected. The layers are less distinguishable than DST2, which contains the same ratio of TiO_2.

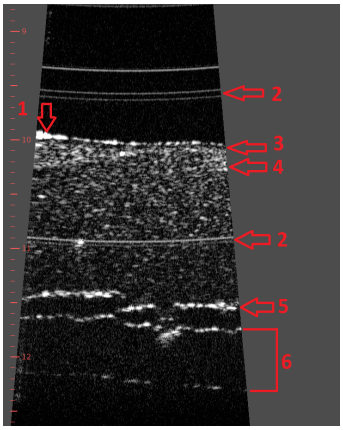

(a) *OCT image of DST2 sample indicating horizontal artefacts (arrows 2), air-tissue interface artefact (arrows 1, 5), tape (location 6) and the urothelium (arrow 3), lamina propria (arrow 4) and muscularis propria (between arrows 4 and 5) layers.*

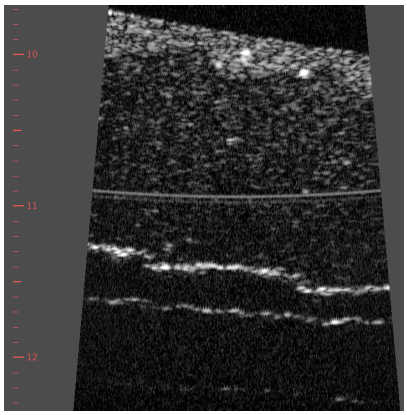

(b) *OCT image of sample DST1, the lamina propria and muscularis propria are distinguishable, no urothelium layer. Saw tooth pattern clearly visible.*

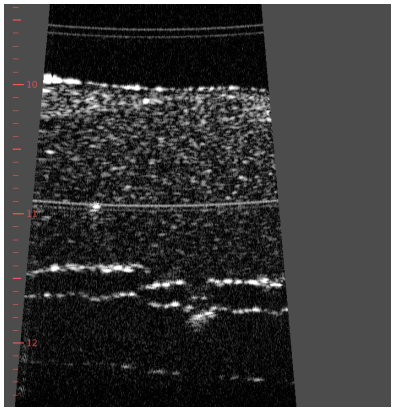

(c) *OCT image of sample DST2. The urothelium, lamina propria and muscularis propria are distinguishable.*

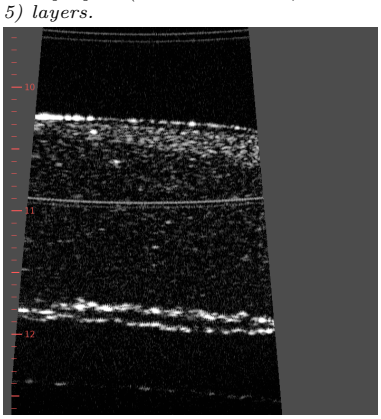

(d) *OCT image of sample DST3. The urothelium, lamina propria and muscularis propria are distinguishable.*

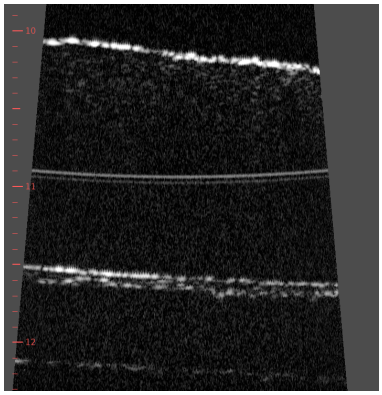

(e) *OCT image of sample DSS. No separate layers are visible. The outlining of the phantom and tape are both visible.*

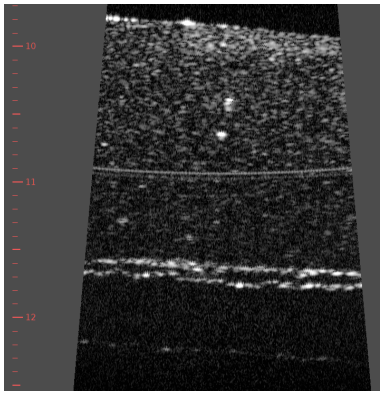

(f) *OCT image of sample EFT. The lamina propria and muscularis propria are visible.*

Figure 13: *Lower bladder samples DST1, DST2, DST3, DSS and EFT imaged with OCT. In the samples where layers are visible (all samples except DSS) a saw tooth pattern is visible. Artefacts are visible in all samples.*

In the samples DST2 and DST3 the urothelium was visible. Therefore only for these samples the thickness of the urothelium and lamina propria was measured. For DST2 the thinnest part of the lamina propria was 170 ± 2 μm and the urothelium was of 60 ± 6.5 μm thick. For DST3 the thinnest part of the lamina propria was 117 ± 12.5 μm and the urothelium was 38 ± 3 μm thick. The correlation between the thickness and spin speeds are visible in figure 14. The trendline had a slope of -0.1534 μm/rpm.

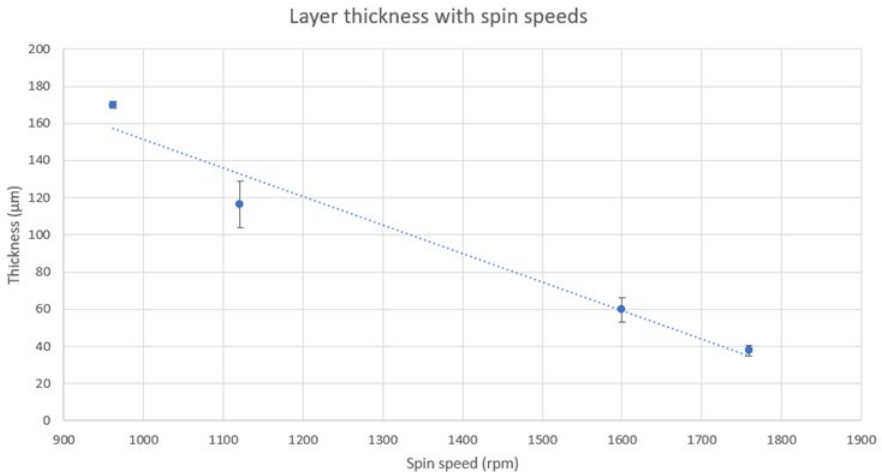

Figure 14: *Spin speeds (rpm) of motor with thickness (µm) of lamina propria and urothelium layers with error bars. Trendline with a slope of -0.1534 µm/rpm.*

5.3 Phantoms

Two phantoms were developed using Dragon skin and TiO_2, this resulted from the OCT images of the samples. In both phantoms the artefacts indicated with arrow 1 and 2 in figure 13a are visible. In phantom BP1 different inks and techniques were tested to develop tumours, see figure 15a. In the second phantom, called BP2, the technique with the least amount of air bubbles and smoothest surface was applied to create the CIS, Ta, T1 and T2 tumour sites, see figure 15b. The sandwich molding production step was done in two parts in both phantoms. In figures 15a and 15b indicated with the red arrows it is visible that there is not a homogeneous base.

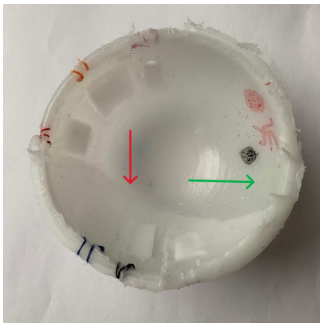

(a) Phantom BP1 with inks and tumour sites. Green arrow indicates location of green ink next to black and red ink locations. The colour labels on the top of the phantom indicate the tumour sites. Red arrow indicates MP transition.

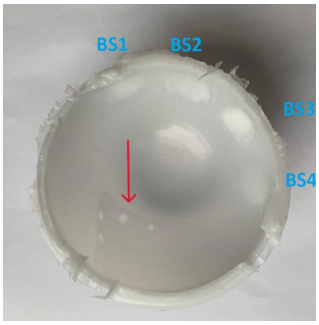

(b) Phantom BP2 with the MP transition with airbubbles indicated with the red arrow. In addition, tumours BS1, BS2, BS3 and BS4 are indicated.

(c) Both the phantoms BP1 (top) and BP2 (bottom).

Figure 15: *Images of the BP1 and BP2 phantoms where certain characteristics like ink locations and tumour sites are indicated.*

In the BP1 phantom black, green and red inks were tested with the OCT system, see figure 16. Green ink

did not dry completely on the phantom. Where black ink is added on the phantom, the shadowing artefact is visible, see figure 16a. With green ink only the shadowing artefact beyond the lamina propria is visible, see figure 16b. Red ink shows no shadowing artefact, see figure 16c.

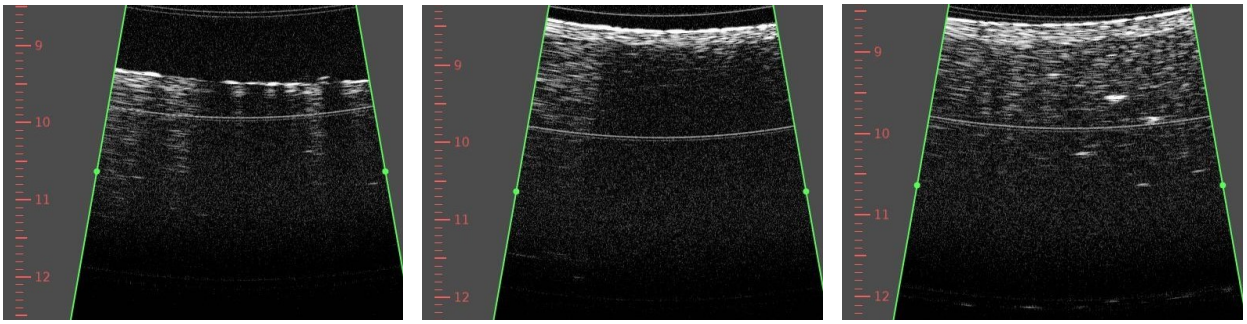

(a) OCT image of a dot with black ink. Most of the intensity is lost.

(b) OCT image of dot with green ink. The intensity of the muscularis propria layer is lost.

(c) OCT image of a dot with red ink. The intensity is only lost at very small parts, but that is negligible.

Figure 16: *OCT images of phantom BP1 with dots of black, green and red inks. The inks have different influences on the data of the OCT image.*

In phantom BP1 different techniques to create different kinds of tumours were tested, see figure 15a. Visually, the cutout tape technique for tumour ZT gave too much structure around the tumour and the adjacent tumours. The tape over technique for tumour PT produced multiple air bubbles. Doing two different tumours next to each other (WT and ZT; OT and RT) resulted in an uneven distribution of material for both tumours. The technique to fill up one spot, flattening it and letting it dry gave the smoothest spot, as in BT.

In phantom BP2, three layers were created. On the OCT images only three layers were visible on a limited number of locations where the air-tissue interface artefact was not present [37], indicated with the arrow in figure 17b. Two main layers were visible on the biggest part of phantom BP2, as in figure 17c. Compared to the porcupine bladder wall (figure 17a), the phantom does show at least two separate layers. A big difference is that the muscularis propria is striated compared to the phantom.

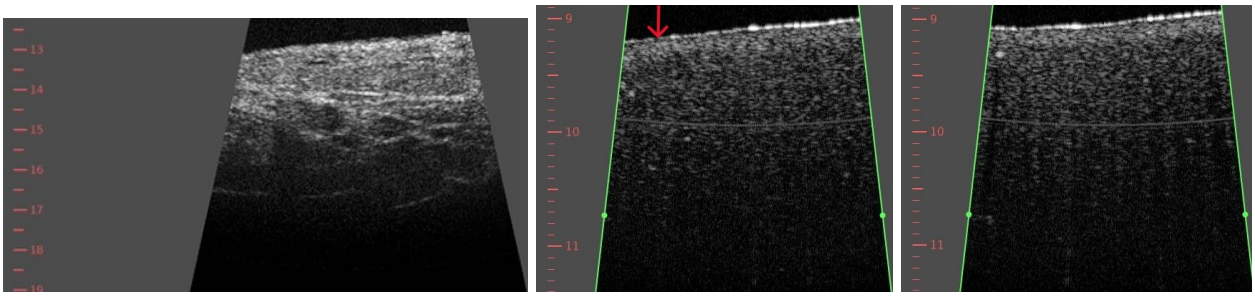

(a) OCT image of porcupine bladder with healthy tissue. In the muscularis propria layer a striated pattern is visible. This image is acquired from the Next gen in-vivo project.

(b) OCT image of the middle of the phantom, at the location of the arrow the thin urothelium layer is distinguishable from the lamina propria layer (red arrow). On the right side of the top of the phantom the air-tissue interface artefact is visible [37].

(c) OCT image of the middle of the phantom where only 2 layers are visible, the whole part of the top is the air-tissue interface artefact visible. No urothelium layer is visible.

Figure 17: *OCT images of porcupine bladder with healthy tissue (a). OCT images of phantom BP2 of the middle of the phantom where the phantom is healthy, so no tumours present (a,b).*

In phantom BP2 the best techniques for tumour sites (CIS, Ta, T1 and T2) were used and OCT images were obtained. For each tumour the transition from the normal layers to tumour layers and a part of the tumour is presented in figure 18. Big and small lumps of TiO_2 are visible in almost all images.

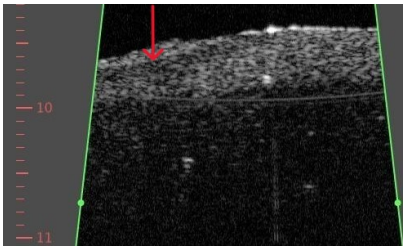

(a) OCT image of the transition to the CIS tumour location (BS1). Several lumps of TiO_2 are visible. Four layers are visible indicated with the red arrow.

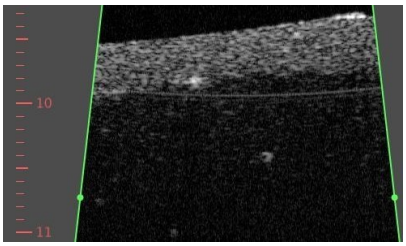

(b) OCT image of CIS tumour site (BS1). Only 2 layers visible, the lamina propria and muscularis propria.

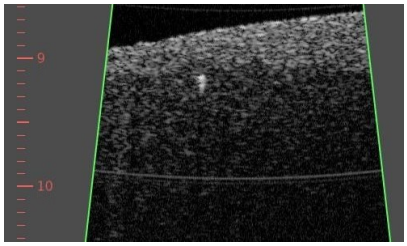

(c) OCT image of transition to the T1 tumour site (BS2), visible by the thickening combined urothelium and lamina propria layer. 2 layers are visible.

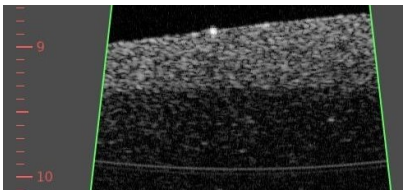

(d) OCT image of the T1 tumour site (BS2) with a clear division of the 2 layers.

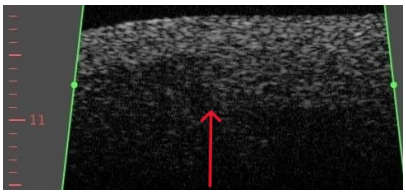

(e) OCT image of the transition to the T2 tumour location (BS3). A sharp edge is visible where the excision was made. On left side of edge clearly 2 layers visible and right side of edge the layers are indistinguishable.

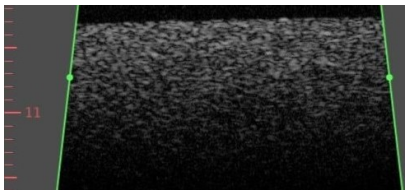

(f) OCT image of T2 tumour location (BS3). An even distribution is visible and no layers are distinguishable.

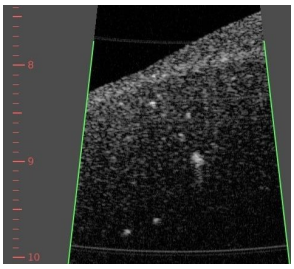

(g) OCT image of transition to the Ta tumour site (BS4). Several TiO_2 lumps are visible.

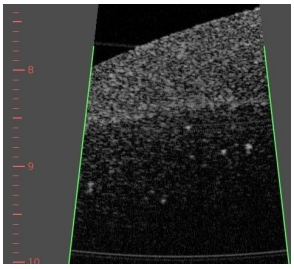

(h) OCT image of Ta tumour (BS4). 3 layers are distinguishable: a very thick urothelium, a lamina propria and a muscularis propria. Again several lumps are visible in the image.

Figure 18: *OCT images of phantom BP2 of the specific tumour sites and transitions of CIS (a, b), T1 (c, d), T2 (e, f) and Ta (g, h) tumours.*

In the OCT images of the CIS tumour, two layers are visible: the lamina propria and muscularis propria, see figure 18b. The transition from the normal phantom layers to the CIS tumour is not completely smooth and a thin lower intensity layer of the urothelium is visible on the left side, indicated with the red arrow in figure 18a. On the OCT images of the T1 tumour a smooth transition is visible, see figure 18c. The two layers of the combined urothelium and lamina propria layer and the separate muscularis propria are visible, see figure 18d. The light penetrates deeper into the phantom than the CIS images. The OCT images of the T2 tumour show an abrupt transition, where the location of the incision is clearly visible, see red arrow in figure 18e. The layers as in a T2 tumour are indistinguishable, see figure 18f. The OCT images of the Ta tumour show a smooth transition of the normal layers to the tumour location. The lamina propria layer stays visible beneath the whole tumour, clearly visible in both figures 18g and 18h. A thick urothelium layer is achieved in this tumour location. In the T1 and Ta tumour sites the light penetrates deeper than in the CIS and T2 images. Figure 19 shows that the OCT images sometimes have a low intensity signal, but this is negligible. The bottom of the phantom is not visible. All tumours are relatively thick compared to the thickness of the lamina propria of the normal layers.

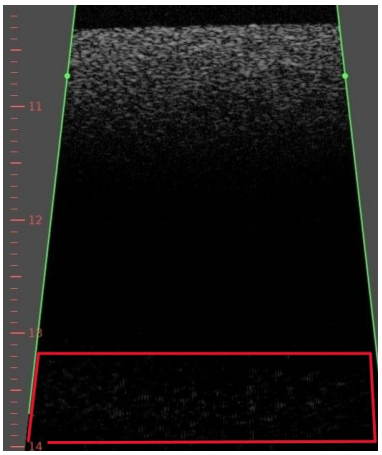

(a) OCT image of T2 tumour. Red box shows where a signal is still visible.

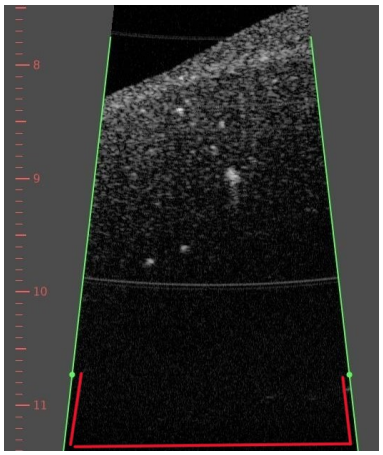

(b) OCT image of Ta tumour. Above red box signal still visible.

Figure 19: *OCT images of T2 (left) and Ta tumour (right). Shows that not enough light penetrates far into the phantom, while some spots with low intensity are sometimes visible.*

5.4 Miniature camera

Using the camera from the Next gen in-vivo project images were acquired of phantom BP2. The images were easy to make and the blood vessels were clearly visible. There are no different colours or structures visible as in a WLC image, see figure 20a [19]. The images from the tumour sites in this phantom did not represent the tumours clearly. The blood vessels created in this phantom were on the other hand clearly visible, see figure 20b.

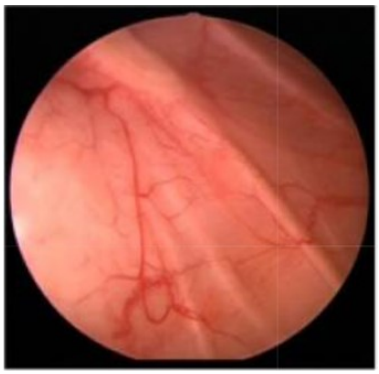

(a) *WLC image of a healthy bladder wall [19]. Several blood vessels are visible.*

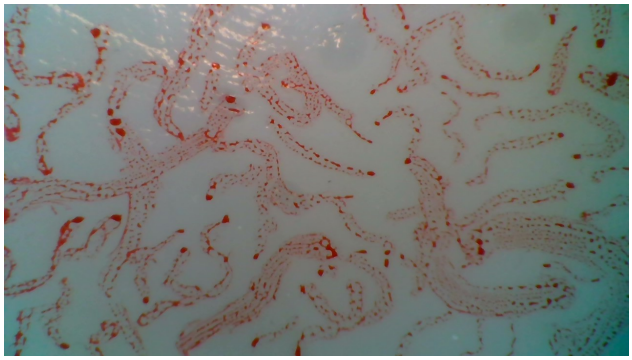

(b) *Image of phantom BP2 with camera recordings. Blood vessels are visible.*

Figure 20: *WLC images of a healthy bladder (left) with visible blood vessels [19] and camera images of phantom BP2 (right).*

6 Discussion

The results presented in Chapter 5 will be discussed below. Several findings will be further explained and elaborated. In addition, the used materials and techniques will be compared and reviewed. Furthermore, limitations, recommendations and further research will be explained and discussed.

6.1 Materials

The samples were made of Ecoflex 00-30 or Dragon skin 10 NV mixed with one of the scatteres, TiO_2 or silica gel. The three layers of the bladder wall could be easily created with certain combinations (except for silica gel) of the materials visible with OCT, complying with requirements TN2, TA1, TR1 and TR3. The materials can be preserved for more than 2 years, meeting requirement TN4. Dragon skin complied with the requirement TPH2. Dragon skin and Ecoflex were suitable materials to work with and both could be analysed with OCT. TiO_2 showed clear distinguishable layers in contrast to silica gel that showed no layers.

Ecoflex 00-30 has a pot life of 75 minutes and a curing time of 4 hours [33]. For sandwich molding, for the muscularis propria, the material was easy to use. However, for spin coating, which was used for the urothelium and lamina propria, breaks were taken between the production of the two layers to prevent overheating of the power supply. This took a lot of time in the production process. Another silicone material or another type of Ecoflex can be used with a shorter curing time to prevent overheating of the power supply. But this can result in different properties of the material, like elasticity.
In contrast with Ecoflex, Dragon skin 10 NV had a shorter pot life of 15 minutes and a curing time of 75 minutes [35]. This material was used in the samples, phantoms and tumour sites. With spin coating and tumour sites there was sufficient time before the material started curing. However, for sandwich molding the time was not enough to be able to cover a large surface. So, this technique was done in two parts, because after the first time the entire mold was not completely filled or large air bubbles could be seen because the material was already curing before everything slid down. In the OCT images a transition of the two parts made with sandwich molding was not visible since the same scatterer ratios were used. The disadvantage was that it delayed the process. To be able to prevent this, a material with a curing time of at least 20 minutes can be used. This could be a better option for creating gradients as well because that also takes time.

For the scatterer ratios of the samples DST3 and DSS an error was made that led to lower %w/w of TiO_2 and silica gel. This probably led to lower intensities of the layers in both samples. The scattering coefficient from the research of Ntombela et al. [27] was mistaken as the attenuation coefficient in the research of de Bruin et al. [22]. The %w/w of TiO_2 and silica gel should therefore be higher because the attenuation coefficient is the scattering coefficient together with the absorption coefficient, $\mu = \mu_a + \mu_s$ [18]. Even though there are clear results in the first OCT scan, further research should be conducted to check whether changing this ratio will change the results and show that silica can be used with OCT. So for silica gel a probably higher %w/w could be used to test if it is a scatterer that can be used with OCT. However, a lot more material would be needed compared to TiO_2 to achieve the same kind of results because of the lower refractive index of silica gel [22]. Secondly, for TiO_2 very small volumes were required which could lead to errors in measurements. There was not enough material of the silicone rubbers to be able to work in bigger volumes, but this would be recommended for further research. A disadvantage of TiO_2 was that several lumps are visible in the OCT images. This can happen if the container was for example not correctly stored or not correctly used. To reduce the amount of lumps in the material a container with a rough structured small piece on the bottom was used. To further reduce these lumps, more of these rough structures could be used. This can be created by using a different container or adding more of these structures into containers with for example hot glue.

On the bladder phantoms different kinds of ink were tested to create blood vessels. This meets requirement TN3 and half of requirement TA8. The red permanent marker had the least influence on the OCT images. This is because the spectrum of light of OCT is around near-infrared light [18]. When black ink is used part of this light is absorbed which results in a shadowing artefact. Which means that not enough

photons are backscattered to create a visual image [38]. The red ink did not have influence on the OCT images, but could be visually improved by choosing another type of ink that sticks better to the silicone, because this permanent marker accumulated in several dots instead of a constant line.

6.2 Techniques

To create layers and tumour sites several techniques were used. To create the base of the phantom sandwich molding and spin coating were used to create three separate layers. For both techniques molds were used that meet requirements TA3 and TA7. By using spin coating the requirements TA1, TA2, TR2 and TR3 were met. And the requirement TPA was met with the created tumour sites. These techniques and requirements are partially discussed in paragraph 3.2.

Spin coating was used to create the urothelium and lamina propria. The measurements of this spin coater that was created in this project can be further improved. The samples DST2 and DST3 showed three layers, but in the phantoms this was almost not visible. Presumably because the layer was too thin and thereby overlapping with the refractive effects of the air-tissue interface artefact [37]. That the layer was too thin could have happened because of an error in the measurement of spin speeds and thickness measurements. The measurements to determine the spin speeds of the setups could be improved by increasing the amount of data points that would result in more accurate slopes for both setups. This applies to the measurements of the thickness of the urothelium and lamina propria in the samples as well, more data points on more locations of the samples are required to have a more accurate correlation.

6.3 OCT images

Two scan moments were used to make the OCT images of the samples and phantoms. The OCT images showed several artefacts. Several of these artefacts were discussed with Scinvivo that built the OCT setup. In addition, the phantom BP2 was compared with a healthy porcupine bladder.
The healthy part of phantom BP2, location with no tumour sites, was compared to a healthy porcupine bladder. This showed that the muscularis propria layer is striated in a normal bladder wall. In further research, experiments could be done by using gradients with different scattering ratios to achieve the same patterns.
Next, the causes of the artefacts on the OCT images of the phantoms and samples, were discussed with Scinvivo. Firstly, there was a horizontal artefact that was constant over all images. This was caused by an error in the system of the OCT probe, this error resulted in an error in the A-line of the OCT. And since B-scans and C-scans are sequences based on A-lines, this is visible as lines in both scans. These artefacts can be reduced by optimising the OCT system. Secondly, air-tissue interface artefacts were visible. This is caused by the big difference in reflective index of the air and material, which causes the bright, white dots [37]. As discussed with Scinvivo, this artefact is difficult to reduce. Lastly, the artefact that was visible when different inks were tested, is called the shadowing artefact. This was caused by a blockage of the beam from the OCT. This blockage results in the beam that cannot reach deeper layers and therefore gives low intensity, "shadowing" [38]. In these experiments with different colours of ink, the blockage was caused by the absorption of the near infrared light beam by the green or black ink.

6.4 Tumour sites

In both phantoms BP1 and BP2 tumours were created and tested. The best tumour techniques in phantom BP1 were also incorporated into phantom BP2. In the OCT images of the tumour sites of phantom BP2 it was visible that all tumour layers are too thick. This prevents the OCT beam from reaching far into the phantom and it is not realistic compared to earlier findings [4]. This could be solved in further research by scraping off the excess material with a curved piece of hard plastic for example. Furthermore, as stated in paragraph 6.1, working with bigger volumes would reduce the possible error in the ratios of the scatterers between the different layers and tumour sites. Small amounts of material were used because the material

was running out, but when possible it is recommended to use normal to bigger volumes.
For the separate tumours in phantom BP2, some notes can be concluded. For the CIS tumour site in figure 18a, four layers were visible. This was presumably caused by a combination of material that was accumulated against or got under the tape and then filled up wider than the hole that was created. This could be prevented by testing different types of tape that stick better, because the tape used did not stick adequately to the silicone material. Another improvement in the tumour sites can be done for the T1 tumour. The only difference between T1 and CIS was the ratio of the scatterer. The only visible difference is that more photons of the OCT beam penetrate the tumour deeper in the T1 tumour than the CIS tumour. This difference is difficult to compare when only one of the two is present. To be able to differentiate these two tumours, it is possible to add a gradient in the urothelium and lamina propria layer of the T1 tumour, where both are present but not distinguishable anymore [4].

6.5 Phantom suggestions

In paragraph 3.1 several requirements and wishes were stated. To be able to improve the current phantom design, some suggestions will be made in this paragraph.
Several details were added to be able to see certain characteristics of the bladder on the miniature camera. Green, black and red inks were tested. To be able for the phantom to appear more as the bladder for the images with the miniature camera, more inks can be tested. There can be experimented with different colours of red and pink whether or not they show a shadowing artefact. Pink can be used in the base and red for the blood vessels [28]. In addition, for the miniature camera some improvements might be added. To make the tumours more realistic for the camera images, a little darker tone might be added to the tumour material visible in figure 5. Furthermore, for the blood vessels different techniques can be tested like the wires as explained in paragraph 2.5.2 [24]. To be able to represent the bladder more in anatomy different shapes can be tested with the spin coater. Generally spin coating is done with rotational symmetrical shapes to prevent hypercoating or hypocoating, but asymmetrical shapes can be possible [19].
More wishes were explained in paragraph 3.1, these can be also used as suggestions for future research. Like improving the anatomy of the bladder by making a more realistic shape (requirement TA4), making openings for the ureters and a urethra (TA5 and TA6), making creases on the wall of the bladder (TA9) or making the phantom so it can hold fluids (TPH1).

6.6 Further research

Next to the already discussed suggestions in the last paragraph, future research can be done to improve the used materials and methods. This was already discussed in detail in this Chapter, a short summary will be presented here with the most important points of improvement. Different techniques and materials were used to create the samples and phantoms. Ecoflex and Dragon skin were used as the base. Dragon skin was the most suitable of the two materials, because it has a short curing time and elastic properties that are similar to that of the bladder wall. More research can be done by looking for a similar material that has a little longer pot life to be able to make tumours and use sandwich molding. Another type of ink can be tested that stays on better on the silicone material. Furthermore, to be able to see the layers on the OCT, TiO_2 was the most suitable scatterer. But the method could be improved to reduce the amount of lumps in the material. In addition, bigger volumes can be used to reduce the possibilities of errors in measuring the scatterers. Lastly, the precise shelf life of the materials needs to be monitored.
To create the phantoms, spin coating was one of the techniques used to create the layers of the bladder wall. For spin coating more research needs to be done to more accurately determine the spin speeds for a certain thickness.
Finally, the tumour sites can be improved by making thinner sites that should result in OCT images that penetrate the phantom deeper. Thinner sites can be acquired by using a curved material, like hard plastic, to remove excess. In addition, a gradient should be added in the T1 tumour to be able to distinguish it from the CIS tumour.

7 Conclusion

For the development of the bladder phantom for the ex-vivo experiment in the Next gen in-vivo project a short literary study was done and 5 pairs of samples and 2 phantoms were created. The samples and phantoms were analysed by OCT and a phantom by the miniature camera. From the results of the literary research the silicone rubber materials Ecoflex and Dragon skin and the scatterers TiO_2 and silica gel were chosen to develop samples analysed with OCT. Based on the results of the samples, Dragon skin and TiO_2 were most suitable to develop the phantoms.
The techniques that resulted from the literary study were sandwich molding for the thicker muscularis propria layer and spin coating for the thinner lamina propria and urothelium layers. A spin coater was designed and created to be able to make these thin layers, to make it possible to see all layers on an OCT image. These techniques are suitable to partially create the anatomy, physiology and pathology of a bladder.
For the development of a bladder phantom in this research, 5 pairs of samples and 2 phantoms were created. Dragon skin together with TiO_2 with a ratio of 0.06 : 0,21 : 0.15 for the urothelium, lamina propria and muscularis propria respectively, gave a clear representation of the three layers, where all layers were distinguishable on OCT. These properties and materials were used for making the bladder phantoms. CIS, T1, T2 and Ta tumours were created in these bladder phantoms. Although the tumours were visible on OCT with their characteristics, there is still room for improvement with regards to thinner tumour layers.
Lastly to be able to make blood vessels to be analysed with the miniature camera from the Next gen in-vivo project a red permanent marker can be used. This type of ink has a negligible influence on the OCT images. Further research can be done to develop a bladder phantom more accurately. This can be done by researching a more suitable material than Dragon skin that has a longer pot life, not too long curing time and still has the properties of the bladder. Furthermore, different pink and red inks can be further tested to create more realistic bladder colours for the miniature camera. And a method to reduce the amount of lumps in the material can be investigated.

In conclusion, a bladder phantom with tumour sites out of Dragon skin and TiO_2 made with sandwich molding and spin coating and inked with red permanent marker is able to be analysed with OCT and a miniature camera used in the Next gen in-vivo project.

References

[1] Bladder cancer – IARC; 2023. [Online; accessed 17. May 2023]. Available from: https://www.iarc.who.int/cancer-type/bladder-cancer/.

[2] Babjuk M, Burger M, Capoun O, Cohen D, Compérat EM, Dominguez Escrig JL, et al. European Association of Urology Guidelines on Non–muscle-invasive Bladder Cancer (Ta, T1, and Carcinoma in Situ). Eur Urol. 2022 Jan;81(1):75–94. doi:10.1016/j.eururo.2021.08.010.

[3] Raharja PAR, Hamid ARAH, Mochtar CA, Umbas R. Recent advances in optical imaging technologies for the detection of bladder cancer. Photodiagn Photodyn Ther. 2018 Dec;24:192–197. doi:10.1016/j.pdpdt.2018.10.009.

[4] Sung HH, Scherr DS, Slaton J, Liu H, Feeny KL, Lingley-Papadopoulos C, et al. Phase II multi-center trial of optical coherence tomography as an adjunct to white light cystoscopy for intravesical real time imaging and staging of bladder cancer. Urologic Oncology: Seminars and Original Investigations. 2021 Jul;39(7):434.e23–434.e29. doi:10.1016/j.urolonc.2021.03.026.

[5] Robotics, Mechatronics. Next Gen In-Vivo Cancer Diagnostics;. [Online; accessed 17. May 2023]. Available from: https://www.ram.eemcs.utwente.nl/research/projects/nextgeninvivo.

[6] Scinvivo. Making cancer obvious;. [Online; accessed 5. Jun. 2023]. Available from: https://www.scinvivo.com.

[7] Hoehn K, Marieb EN. Human Anatomy & Physiology. 10th ed. PEARSON EDUCATION Limited; 2016.

[8] Bolla SR, Odeluga N, Amraei R, Jetti R. Histology, Bladder. In: StatPearls [Internet]. StatPearls Publishing; 2023. Available from: https://www.ncbi.nlm.nih.gov/books/NBK540963.

[9] Bovenkamp D, Sentosa R, Rank E, Erkkilä MT, Placzek F, Püls J, et al. Combination of High-Resolution Optical Coherence Tomography and Raman Spectroscopy for Improved Staging and Grading in Bladder Cancer. Appl Sci. 2018 Nov;8(12):2371. doi:10.3390/app8122371.

[10] Anatomy of the Bladder - Health Encyclopedia - University of Rochester Medical Center; 2023. [Online; accessed 17. May 2023]. https://www.urmc.rochester.edu/encyclopedia/content.aspx?contenttypeid=34contentid=BBlaO2.

[11] Chalana V, Dudycha S, Yuk JT, McMorrow G. Automatic Measurement of Ultrasound-Estimated Bladder Weight (UEBW) from Three-Dimensional Ultrasound. Reviews in Urology. 2005;7(Suppl 6):S22–S28.

[12] Li C, Guan G, Zhang F, Song S, Wang RK, Huang Z, et al. Quantitative elasticity measurement of urinary bladder wall using laser-induced surface acoustic waves. Biomed Opt Express. 2014 Dec;5(12):4313–4328. doi:10.1364/BOE.5.004313.

[13] Davis NF, Mulvihill JJE, Mulay S, Cunnane EM, Bolton DM, Walsh MT. Urinary Bladder vs Gastrointestinal Tissue: A Comparative Study of Their Biomechanical Properties for Urinary Tract Reconstruction. Urology. 2018 Mar;113:235–240. doi:10.1016/j.urology.2017.11.028.

[14] Kaseb H, Aeddula NR. Bladder Cancer. In: StatPearls [Internet]. StatPearls Publishing; 2022. Available from: https://www.ncbi.nlm.nih.gov/books/NBK536923.

[15] Schmidbauer J, Remzi M, Klatte T, Waldert M, Mauermann J, Susani M, et al. Fluorescence Cystoscopy with High-Resolution Optical Coherence Tomography Imaging as an Adjunct Reduces False-Positive Findings in the Diagnosis of Urothelial Carcinoma of the Bladder. Eur Urol. 2009 Dec;56(6):914–919. doi:10.1016/j.eururo.2009.07.042.

[16] Lerner SP, Goh AC, Tresser NJ, Shen SS. Optical Coherence Tomography as an Adjunct to White Light Cystoscopy for Intravesical Real-Time Imaging and Staging of Bladder Cancer. Urology. 2008 Jul;72(1):133–137. doi:10.1016/j.urology.2008.02.002.

[17] Schoeb DS, Wollensak C, Kretschmer S, González-Cerdas G, Ataman C, Kayser G, et al. Ex-vivo evaluation of miniaturized probes for endoscopic optical coherence tomography in urothelial cancer diagnostics. Annals of Medicine and Surgery. 2022 May;77:103597. doi:10.1016/j.amsu.2022.103597.

[18] Boudoux C. Fundamentals of biomedical optics: From light interactions with cells to complex imaging systems. 1st ed. Pollux, Montréal; 2017.

[19] Smith GT, Lurie KL, Khan SA, Liao JC, Ellerbee AK. Multilayered disease-mimicking bladder phantom with realistic surface topology for optical coherence tomography. In: Nordstrom RJ, Bouchard JP, Allen DW, editors. Design and Performance Validation of Phantoms Used in Conjunction with Optical Measurement of Tissue VI. vol. 8945. International Society for Optics and Photonics. SPIE; 2014. p. 89450E. Available from: https://doi.org/10.1117/12.2036402. doi:10.1117/12.2036402.

[20] Pearce S, Daneshmand S. Enhanced Endoscopy in Bladder Cancer. Curr Urol Rep. 2018 Oct;19:84. doi:10.1007/s11934-018-0833-9.

[21] Zulina N, Caravaca O, Liao G, Gravelyn S, Schmitt M, Badu K, et al. Colon phantoms with cancer lesions for endoscopic characterization with optical coherence tomography. Biomed Opt Express. 2021 Feb;12(2):955–968. doi:10.1364/BOE.402081.

[22] de Bruin DMM, Bremmer RH, Kodach VM, de Kinkelder R, van Marle J, van Leeuwen TG, et al. bruins with controlled optical properties. Journal of Biomedical Optics. 2010;15(2):025001. Available from: https://doi.org/10.1117/1.3369003. doi:10.1117/1.3369003.

[23] Lee HJ, Samiudin NM, Lee TG, Doh I, Lee SW. Retina phantom for the evaluation of optical coherence tomography angiography based on microfluidic channels. Biomed Opt Express. 2019 Nov;10(11):5535–5548. doi:10.1364/BOE.10.005535.

[24] Smith GT, Lurie KL, Zlatev DV, Liao JC, Bowden AKE. Multimodal 3D cancer-mimicking optical phantom. Biomed Opt Express. 2016 Feb;7(2):648–662. doi:10.1364/BOE.7.000648.

[25] Chang S, Handwerker J, Giannico GA, Chang SS, Bowden AK. Birefringent tissue-mimicking phantom for polarization-sensitive optical coherence tomography imaging. vol. 27. Society of Photo-Optical Instrumentation Engineers; 2022. p. 074711. doi:10.1117/1.JBO.27.7.074711.

[26] Choi E, Waldbillig F, Jeong M, Li D, Goyal R, Weber P, et al. Soft Urinary Bladder Phantom for Endoscopic Training. Ann Biomed Eng. 2021 Sep;49(9):2412–2420. doi:10.1007/s10439-021-02793-0.

[27] Ntombela L, Adeleye B, Chetty N. Low-cost fabrication of optical tissue phantoms for use in biomedical imaging. Heliyon. 2020;6(3):e03602. Available from: https://www.sciencedirect.com/science/article/pii/S2405844020304473. doi:https://doi.org/10.1016/j.heliyon.2020.e03602.

[28] Smith GT, Lurie KL, Khan SA, Liao JC, Ellerbee AK. Multilayered disease-mimicking bladder phantom with realistic surface topology for optical coherence tomography. In: Design and Performance Validation of Phantoms Used in Conjunction with Optical Measurement of Tissue VI. vol. 8945. SPIE; 2014. p. 101–108. doi:10.1117/12.2036402.

[29] Hacker L, Wabnitz H, Pifferi A, Pfefer TJ, Pogue BW, Bohndiek SE. Criteria for the design of tissue-mimicking phantoms for the standardization of biophotonic instrumentation. Nat Biomed Eng. 2022 May;6:541–558. doi:10.1038/s41551-022-00890-6.

[30] Bykov A, Popov A, Kinnunen M, Prykäri T, Priezzhev A, Myllylä R. Skin phantoms with realistic vessel structure for OCT measurements. Proceedings of SPIE - The International Society for Optical Engineering. 2010 june;7376:73760F. doi:10.1117/12.872000.

[31] Ishii T, Ho CK, Nahas H, Yiu BYS, Chee AJY, Yu ACH. Deformable phantoms of the prostatic urinary tract for urodynamic investigations. Med Phys. 2019 Jul;46(7):3034–3043. doi:10.1002/mp.13558.

[32] Lamouche G, Kennedy BF, Kennedy KM, Bisaillon CE, Curatolo A, Campbell G, et al. Review of tissue simulating phantoms with controllable optical, mechanical and structural properties for use in optical coherence tomography. Biomed Opt Express. 2012 Jun;3(6):1381–1398. doi:10.1364/BOE.3.001381.

[33] Smooth-on. Ecoflex™ Series;. Accessed on May 23, 2023. Available from: https://www.smooth-on.com/product-line/ecoflex/.

[34] Smooth-on. Dragon Skin™ Series, High Performance Silicone Rubber;. [Online; accessed 10. Jun. 2023]. Available from: https://www.smooth-on.com/product-line/dragon-skin.

[35] Smooth-on. Dragon Skin™ 10 NV;. Accessed on May 23, 2023. Available from: https://www.smooth-on.com/products/dragon-skin-10-nv/.

[36] Ejofodomi OA, Zderic V, Zara JM. Tissue-mimicking bladder wall phantoms for evaluating acoustic radiation force—optical coherence elastography systems. Med Phys. 2010 Apr;37(4):1440–1448. doi:10.1118/1.3352686.

[37] Golabchi A, Faust J, Golabchi F, Brooks D, Gouldstone A, Dimarzio CA. Refractive errors and corrections for OCT images in an inflated lung phantom. Biomedical optics express. 2012 05;3:1101–9. doi:10.1364/BOE.3.001101.

[38] Anvari P, Ashrafkhorasani M, Habibi A, Falavarjani KG. Artifacts in Optical Coherence Tomography Angiography. Journal of Ophthalmic & Vision Research. 2021 Apr;16(2):271–286. doi:10.18502/jovr.v16i2.9091.